NASA CONTRACTOR REPORT

NASA CR-1740

EXPERIMENTAL INVESTIGATION OF THE NONEQUILIBRIUM RADIATION EMITTED BY MARS-LIKE GAS MIXTURES

by Jackie O. Bunting

Prepared by
MARTIN MARIETTA CORPORATION
Denver, Colo. 80201
for Langley Research Center

NATIONAL AERONAUTICS AND SPACE ADMINISTRATION • WASHINGTON, D. C. • JANUARY 1971

1. Report No.	2. Government Accession No.	3. Recipient's Catalog No.
NASA CR-1740		

4. Title and Subtitle	5. Report Date
EXPERIMENTAL INVESTIGATION OF THE NONEQUILIBRIUM RADIATION EMITTED BY MARS-LIKE GAS MIXTURES	January 1971
	6. Performing Organization Code

7. Author(s)	8. Performing Organization Report No.
J. O. Bunting	MCR-70-155
	10. Work Unit No. 124-07-14-01-23

9. Performing Organization Name and Address	11. Contract or Grant No.
Martin Marietta Corporation Denver Division Denver, Colorado 80201	NAS 1-9471
	13. Type of Report and Period Covered

12. Sponsoring Agency Name and Address	14. Sponsoring Agency Code
National Aeronautics and Space Administration Washington, D.C. 20546	

15. Supplementary Notes

16. Abstract

The spectral radiative intensity has been measured under various test conditions for three different candidate Mars atmospheres over the wavelength range from 0.275 to 5.0 microns. The infrared portion of the spectral radiation for all three gas mixtures tested show a peak in intensity between 4.3 and 5.0 microns corresponding to the fundamental rotation-vibration band of CO_2 and the 5.0 micron bands of CO_2. The 100 percent CO_2 test gas also shows a strong band radiation at 2.7 microns and this strong peak is greatly reduced when either nitrogen or argon are added to the test gas mixture. The nonequilibrium radiation that appears in the infrared always occurs in those spectral regions for which the equilibrium levels are lowest. Maximum observed nonequilibrium overshoots occur in the visible portion of the spectrum and are generally no larger than two times the equilibrium value. The major portion of both the infrared and the visible spectrums have nonequilibrium overshoots less than 1.5 times the equilibrium values.

17. Key Words (Suggested by Author(s))	18. Distribution Statement
Radiative heating, Nonequilibrium radiation, Mars entry heating, Properties of CO_2-N_2-A Gas Mixtures, Spectral radiation of CO_2-N_2-A Gas Mixtures	Unclassified - Unlimited

19. Security Classif. (of this report)	20. Security Classif. (of this page)	21. No. of Pages	22. Price*
Unclassified	Unclassified	34	$3.00

*For sale by the National Technical Information Service, Springfield, Virginia 22151

EXPERIMENTAL INVESTIGATION OF THE NONEQUILIBRIUM RADIATION EMITTED BY MARS-LIKE GAS MIXTURES

By Jackie O. Bunting
Martin Marietta Corporation

SUMMARY

This report describes an experimental investigation conducted by Martin Marietta Corporation to measure the radiation emanating from gas mixtures which are presumed to constitute the Martian atmosphere. Limited analyses and experimental observations have led to the widely recognized fact that CO_2, N_2, A mixtures radiate an order of magnitude more strongly than air in the velocity range of 4 to 5 km/sec. Extrapolation of the existing nonequilibrium radiation data, recorded at velocities above 6 km/sec, can result in serious anomalies, depending upon what data are used and how they are extrapolated.

Martin Marietta's high-performance shock tube was used to generate normal shock waves of various strengths in three different mixtures of CO_2, N_2, and A. The absolute radiative intensity behind the shock front was measured over the wavelength range from 0.25 to 5.00 μ for each gas mixture/shock velocity combination. The measured equilibrium radiation is presented for each series of test conditions and the probable source of the observed radiation is identified. Nonequilibrium radiation levels are presented as ratios of peak overshoot intensities to corresponding equilibrium intensities.

Test gas mixtures containing argon show an unusual second nonequilibrium overshoot, which is associated with the delayed argon relaxation process. In general, the peak nonequilibrium overshoots are no larger than two times the corresponding equilibrium values. In most cases, the large nonequilibrium overshoot occurs at a portion of the spectrum where the equilibrium radiation is already very low.

INTRODUCTION

When existing data on the nonequilibrium radiation of Mars-like gas mixtures in the velocity range 6 to 10 km/sec are extrapolated to velocities appropriate for a Mars orbital entry (4 to 5 km/sec), serious anomalies can result. Depending on what data are used and how they are extrapolated, the relative importance of the nonequilibrium radiation goes from negligible to dominant. The purpose of the present investigation is to eliminate some of this uncertainty through the measurement of the equilibrium and nonequilibrium spectral radiation behind a normal shock wave in three different gas mixtures of CO_2, N_2, and A, corresponding to current estimates of the atmospheric composition of Mars.

An early study which pointed out the possibility of the importance of radiation heat transfer in shocked CO_2, N_2 mixtures was presented by Boobar and Foster (ref. 1). Using analytical techniques, they studied the equilibrium properties of shocked planetary atmospheres and found that the gas radiation was much stronger than the radiation from air at equivalent flight conditions. The principal source of this radiation was the CN violet band system.

James (ref. 2), in an early experimental study using a ballistic range, measured the radiant intensity from the gases in the shock layer of small projectiles for several compositions and deduced that the CN violet system was indeed the dominant emitter for CO_2 lean mixtures in the spectral range between 0.2 and 1.0 μ. These results also presented a first indication of the possible importance of the nonequilibrium radiation, but no quantitative results were presented.

Early shock tube experiments were performed by Fairbairn (ref. 3), Gruszczynski and Warren (ref. 4), and Thomas and Menard (ref. 5). Fairbairn worked in the reflected shock region, and therefore dealt only with equilibrium radiation. His detailed spectral measurements confirmed the dominance of the CN red and violet systems at 8000°K. Other bands found were N_2^+ (1-), N_2(2+), and C_2 (Swan), but these were relatively weak. These results were again restricted to the range between 0.23 and 1.2 μ. Gruszczynski and Warren presented a large amount of radiation data for velocities greater than 30 000 fps, which are too high for application to Mars entry studies. Thomas and Menard gathered data for several mixtures over a large range of velocities in a similar spectral regime by measuring the total radiation flux from the shock layer of a small stationary model mounted in the shock tube. These experiments again showed the dominance of the CN violet system at velocities of about 25 000 fps. In addition, they presented the first quantitative values of the nonequilibrium heat transfer in 9% and 30% CO_2 mixtures at 25 000 fps. These were 55 and 93 W/cm^2, respectively -- loads that are very large when compared to the corresponding conditions for air. During these shock tube experiments, a small amount of data was gathered for the radiative properties of shocked 100% CO_2. Since this radiation was weak compared to the CO_2 lean mixtures in the spectral regime considered, it was not fully investigated.

Arnold, Reis, and Woodward (ref. 6) conducted more refined experiments using a ballistic range. Further evidence was obtained that the CN violet system was dominant, and the variation of the nonequilibrium heat transfer with velocity was found. A comparison of these results and the shock tube results of Thomas and Menard (ref. 5) shows apparent agreement for the 9% CO_2 mixture at 25 000 fps, but shows a factor of three disagreement for the 30% CO_2 mixture. Even this modest agreement may be fortuitous, as conflicting values of D_o^o, the energy of dissociation of CN, can be deduced from the two sets of results.

The nonequilibrium data from Thomas and Menard (ref. 5) are not directly comparable to those of Arnold, Reis, and Woodward (ref. 6). The Thomas and Menard equilibrium data resulted in a D_o^o of 7.7 eV, while the Arnold *et al.* equilibrium data as quoted by Reis had D_o^o = 8.2 eV. At 7.5 km/sec, the calculated equilibrium radiation intensity increases by a factor of three in going from 7.7 to 8.2 eV. Rumpel and Deacon (ref. 7) have concluded a value of D_o^o = 7.9 eV after reviewing the experimental results from many sources. More recent experimental data by Reis (ref. 8) and Gruszczynski (ref. 9) suggest a value of 8.1 to 8.2 eV. Thus, the theoretical projection of experimental data at 7.5 km/sec could have I_{NE} varying from 10 to 300 W/cm^2, compared to convective heating rates between 10 to 100 W/cm^2 for velocities between 4.0 and 5.2 km/sec. In other words, analytical projections of existing data result in serious anomalies, and the extrapolation to Mars entry conditions is highly questionable.

A recent attempt to gain better understanding of the chemical kinetics of CO_2, N_2 mixtures was reported by McKenzie and Arnold (ref. 10). Using a combined theoretical and experimental approach, they were able to produce a reasonable kinetic model for predicting the CN violet signature through the nonequilibrium zone behind shock waves moving at velocities above 20 000 fps. However, theory and experiment did not agree at lower velocities, and the actual peak CN violet intensity was less than predicted. It is unfortunate that this work was not reduced to a nonequilibrium heat transfer rate so that some indication of the solution of the discrepancy could be determined. The most recent work which has appeared in the literature is a short article by Menees and McKenzie (ref. 11), in which they were able to predict the CN violet signature at high velocities without going to the complexity of specific collision partners.

From the above discussion of the available work done on the nonequilibrium flow behind the shock waves in CO_2, N_2 mixtures, it is apparent that available knowledge is not adequate to confidently design Mars entry vehicles. All of the available data are dominated by the CN violet band system, perhaps because of the limited spectral regime considered or perhaps because high velocities have received the most attention. In the present work, the test conditions have been selected to give the radiation data required to make heat transfer predictions for a Mars orbital entry vehicle.

SHOCK TUBE FACILITY

Martin Marietta Corporation constructed a pressure-driven, buffered, chambered shock tube (fig. 1) to study problems in gas physics and real gas dynamics associated with the entry of space vehicles into the atmosphere of Earth or any other planet. Several advantages are associated with this tube configuration. The diameter of the buffer is the same as that of the driver, and the area contraction is between the buffer and the driven sections; this allows shock Mach number performance to approach that of combustion-driven tubes without encountering certain of the operational difficulties of combustion drivers. Optimum performance is obtained when hydrogen is used as the driver gas and a low-molecular-weight gas (helium or nitrogen) is used in the buffer.

The driver and buffer sections of the tube are of standard seamless, hot-drawn, mild steel tubing with an inside diameter of 10-1/8 in. The driver is 3 ft long and the buffer is 10 ft long. Each has forged steel flanges screwed to its ends. A weld at the back of each flange serves as a pressure and vacuum seal. Each section is separated by a diaphragm and sealed with O-ring seals. The driven section, made of 4-in.-inside diameter and 5-in.-outside diameter hot-drawn, seamless, mild-steel tubing, consists of two 6-ft lengths, a 3-ft length, and an 18-in. test section. These are machined to accurate internal diameter and honed to a 16-μin. finish.

The test section is equipped with a pair of centrally located, diametrically opposed 3/8-in.-diameter sapphire windows. Three additional ports are provided across the test section for measuring shock velocity.

Downstream of the driven tube, the flow is dumped into a 15-ft-long, 20-in.-diameter tank, or, if it is desired to study conditions behind a reflected shock, a heavy end plate can be bolted to the final driven tube flange. To facilitate diaphragm changes, the heavy buffer section is rigidly mounted on a support table and the driver and driven sections are mounted on rollers.

EXPERIMENTAL TECHNIQUE

Loading the Driven Tube

The driven tube and dump tank are evacuated to a pressure not exceeding 5 μ of mercury. Then the leak rate is checked, and the maximum acceptable pressure increase is taken as 1 μ of Hg in 5 minutes. Next, the test section is purged with test gas, reevacuated, and finally charged to the desired initial pressure. The tube is fired without delay. Initial driven tube pressures are measured with a Cenco 2200 McLeod vacuum gauge.

Measurement of Shock Speeds

Local shock speed at the test section is measured using a pair of high-response piezoelectric pressure transducers to locate the shock front, and a dual-beam oscilloscope to record the time for the shock to travel between the two instruments.

Spectroscopic Survey

Emission measurements in both the visible and IR portions of the spectrum were made using the system shown in figure 2. Radiation from the hot gas behind the incident shock in the test section of the shock tube passes through the sapphire windows and is focused on the entrance slit of each monochromator. Light of the wavelength interval under observation emerges from the monochromator exit slit and is collected by a photomultiplier whose output is recorded on an oscilloscope.

A complete description of the monochromator and the different photomultipliers used in this study is given in the following section.

DATA REDUCTION AND CALIBRATION PROCEDURE

Data Reduction

The data reduction procedure used here for deducing the specific gas intensity from measured monochromator signals is the same as that outlined by Menard and Thomas (ref. 12). The portion of their analysis which follows serves as an introduction to the specific details of the present calibration.

Assuming an optically thin gas and an isotropic radiation source, P_g, the radiant power (W/μ) to the detector at a specific wavelength λ is given as

$$P_g = \xi_\lambda G_\lambda \iiint d\Omega \, dA \, dx, \tag{1}$$

and the power from the standard calibration source is given as

$$P_c = \xi_\lambda N_\lambda \iint d\Omega \, dA, \tag{2}$$

where ξ_λ is a combined parameter containing all transmission losses, monochromator efficiency, and detector sensitivity, G_λ is the specific radiation intensity (W/cm^3-μ-sr) of the gas, Ω is the solid angle where A is the cross-sectional area of the field-of-view rays as defined by the entrance optics, and x is the coordinate along the optical path. N_λ, the intensity (W/cm^2-μ-sr) of the black-body calibration source, is given in terms of the absolute temperature of the cavity by Planck's radiation law:

$$N_\lambda = \frac{C_1}{\lambda^5}\left(\exp \frac{C_2}{\lambda T} - 1\right)^{-1}. \tag{3}$$

C_1 and C_2 are the first and second radiation constants, which are given by Stair, Johnston, and Halback (ref. 13) as:

$$C_1 = 1.19088 \times 10^{-12} \text{ W-cm}^2/\text{sr};$$

$$C_2 = 1.4380 \text{ cm-°K}.$$

Over the linear response range of the photo detectors, the output voltage E is porportional to the input power P. Therefore, by taking the ratio of equations (1) and (2), the specific intensity emitted by the gas at a particular wavelength is given as

$$G_\lambda = K N_\lambda \frac{E_g}{E_c}, \tag{4}$$

where K, the view factor coefficient, is defined by

$$K = \frac{\iint d\Omega \, dA}{\iiint d\Omega \, dA \, dx}. \tag{5}$$

An analytical solution of equation (5) would be very difficult for the particular geometry used in this experiment, so an alternative method is employed to determine K experimentally. Integration of equation (2) over the path length L yields

$$\int_o^L P_c \, dx = \xi_\lambda \, N_\lambda \iiint d\Omega \, dA \, dx. \tag{6}$$

Then, combining equation (6) with equation (1), and once again assuming linear detector response, G_λ is given as

$$G_\lambda = N_\lambda \frac{E_g}{\int_o^L E_c \, dx}. \tag{7}$$

The integral $\int_o^L E_c \, dx$ is obtained experimentally by moving the calibration source along the optical path from 0 to L and integrating a plot of the resulting outputs.

Setting equation (7) equal to equation (4), the constant K is given by

$$K = \frac{E_c}{\int_o^L E_c \, dx}. \tag{8}$$

Although E_c is a function of λ and x, K is only a function of x, as can be seen from equation (5). To determine K for any convenient location, such as x_i, the $\int_o^L E_c \, dx$ need be measured only once at any desired wavelength λ_o. Thus, at x_i:

$$K(x_i) = \frac{E_c(\lambda_o, x_i)}{\int_o^L E_c(\lambda_o, x) \, dx}. \tag{9}$$

After K has been determined as above, G_λ can be computed from equation (4) once $E_c(x_i)$ is known as a function of λ. The measurements of $E_c(x_i)$ vs λ are obtained by placing the calibration source at x_i and measuring the wavelength dependence of the output signal. The only restriction on x_i is that it be within the optical path. For convenience, we have always used the

centerline of the shock tube, where the entrance slit of the monochromator is focused.

Monochromators for Infrared Survey

The infrared gas radiation behind the incident shock wave was monitored by two Perkin-Elmer model 98 calcium fluoride (CaF_2) prism monochromators. The experimental arrangement used is shown in figure 2. Radiation passing through each sapphire exit window of the shock tube is collected by an f/4, 147-mm-focal-length parabolic mirror and focused on the entrance slit of the monochromator.

The spectral slit width for the model 98 monochromator, which depends on the prism material and the physical slit width, has been computed for various prism materials by Gillespie, Avrin, and Ress (ref. 14). Their results, shown in figure 3, are for a CaF_2 prism and a 1-mm physical slit width. Spectral slit widths corresponding to physical slit widths other than 1 mm are obtained by noting that the spectral slit width is directly proportional to the physical slit width.

IR Detectors

The infrared detectors, supplied by the Philco-Ford Corp. as series ISC-301B, are of the photovoltaic type, designed for operation at liquid nitrogen temperatures. The photosensitive element consists of a single crystal of indium antimonide exhibiting a long wavelength cutoff near 6 μ and a short wavelength cutoff somewhat less than 1 μ. Signal response for these detectors is linear up to 1000 W/cm^2, which is well beyond the signal levels encountered in these experiments.

The sensitive area of each detector, 2 mm by 5 mm, restricts the useful slit height to something less than 5 mm but does not restrict slit widths, since the maximum available width is 2 mm and the value used is always less than this maximum. Slit heights are restricted at the entrance of the monochromator by an adjustable masking arrangement. The image of the slit is focused on the sensitive area of the detector by a parabolic mirror, as shown in figure 2.

The time response of the gauges as received from the manufacturer was slightly greater than 10 μsec, thus necessitating a parallel load resistance to lower this value to less than 1 μsec. Because of the resulting decrease in signal level caused by adding this parallel load resistance, it was necessary to use an amplifier with a gain of 100 before feeding the signal into the oscilloscope preamplifier. The rise time of the amplifier, including the preamplifier of the recording oscilloscope, is much less than 1 μsec (∿100 nsec). Hence, the overall rise time of the circuit is limited by that of the detectors; and in both cases, this is less than 1 μsec.

Wavelength Calibration for IR

Wavelength calibration of the Perkin-Elmer monochromators was accomplished by using a combination of narrowband IR filters, a 50-μ film of polystyrene, and the strong absorption band of CO_2 in the atmosphere. The narrowband filters were part of a standard set supplied by Optics Technology, Inc. Figure 4 shows the calibration curves obtained for each instrument.

Absolute Intensity Calibration for IR

The absolute intensity calibration was accomplished using a bench setup, identical to that shown in figure 2, with a black-body cavity located at the centerline of the simulated shock tube. The position of the centerline can be located quite carefully by backlighting the exit slit of the monochromator with a strong diffuse light source and then placing the exit of the black-body cavity at the image of the monochromator entrance slit. The entrance optics are chosen to give a one-to-one magnification of the entrance slit (as viewed from the centerline of the shock tube).

As a precaution against possible damage in shipment, the linearity of the slit opening was checked before the calibration tests by measuring the monochromator output, at a fixed wavelength, for various physical slit widths. Since the output intensity varies as the square of the slit width, a plot of slit width vs the square root of the intensity should define a straight line passing through the origin. Any deviation from this straight line represents an irregularity in the slit opening. Failure to pass through the origin represents an error in the zero setting of the slit width dial.

This check was performed for each instrument, and in both cases, the straight line defined by the data points passed through the origin of the plot well within experimental error limitations.

The black-body source used was operated at a temperature of 1000 ± 2°C with a chopper frequency of 700 cps. Before each run, the cavity was allowed 90 minutes to stabilize, and all tests for a given instrument were accomplished without interruption.

Data points for the curves of $E_c(x_i)$ vs λ were taken with x_i corresponding to the centerline location and a 0.500-mm slit width. Typical results (fig. 5) show two strong absorption lines with centers at 2.75 and 4.26 μ. The line at 2.75 μ represents absorption for a combination of water vapor and CO_2 in the room atmosphere. The line at 4.26 μ is due only to CO_2 absorption.

Figure 6 shows the results of $E_c(x_i)$ vs x_i at fixed λ. These data are taken under the same conditions as were the previous data, with the black body being translated along the optical path via a movable support stand.

The view factors for the two instruments, computed by the method described before, are 0.1015 and 0.1035, respectively. The difference here is less than 2% and an average value of 0.1025 will be used in the computation of G_λ.

A final check on the accuracy of the entire calibration procedure entails an observation of the same experimental event with each instrument and a comparison of the resulting values of G_λ as measured by different instruments. This check has been performed at three different wavelengths and for two different shock velocities. In all cases, the agreement was within 2%, which is quite satisfactory.

Monochromators for the Visible Survey

The radiation between 2700 and 8500 Å was monitored by one Perkin-Elmer model 98 CaF_2 prism monochromator and one Gaertner model L 234-150 quartz prism monochromator. The Gaertner instrument, with an RCA 1P28 photomultiplier, was used for the lower wavelengths between 2700 and 5500 Å, while the Perkin-Elmer instrument, with an RCA 7265 photomultiplier, was used between 5500 and 8500 Å. The Littrow mirror of the Perkin-Elmer instrument was readjusted to allow drum settings to be made in the visible range, and a new wavelength calibration was made using a set of narrowband visible filters. Drum numbers recorded with the Littrow mirror readjusted are shown in figure 4. The Gaertner instrument has a wavelength calibrated drum and it too was checked for accuracy with narrowband visible vilters.

The absolute intensity calibration was accomplished as described for the IR instruments, except that a tungsten filament lamp was used as a standard. This lamp was compared with a primary standard from the National Bureau of Standards.

The entrance optics used were identical with those described previously and the linearity of the slit opening was again varified. View factors as computed from these two calibrations were in good agreement with the quoted value of 0.1025, and a comparison check of the two instruments looking at the same shock front showed good agreement.

SPECTRAL RADIATION RESULTS

Infrared Spectral Survey

Each of the different gas mixtures (100% CO_2, 80% CO_2 - 20% A, and 99% CO_2 - 1% N_2) was surveyed for possible sources of gas radiation in the wavelength region between 1.00 and 5.00 μ. The wavelength step was 0.100 μ, and the spectral slit width was approximately 0.1 μ.

The first three surveys were made with shock velocities between 15 000 and 16 000 fps into 1.0 mm Hg of test gas. A fourth survey was made using 100% CO_2 as test gas and an average shock velocity of 12 640 fps into a test gas with an initial pressure of 2.0 mm Hg. A typical oscillograph record for one shot is shown in figure 7(d), where both traces recorded the same event at different gain settings. This record corresponds to an equilibrium radiation level of 0.227 W/cm^3-μ-sr at a wavelength of 4.26 ± 0.10 μ. Test conditions

for this shot are a shock velocity of 12 864 fps into 2.0 mm Hg of CO_2 test gas. The record shows a clear sharp rise in radiation level at the shock front with no nonequilibrium overshoot.

The remaining equilibrium radiation results of the spectral survey corresponding to shock velocities near 12 640 fps into 2.0 mm Hg of 100% CO_2 test gas are shown in figure 8. As is shown clearly in this figure, there are two regions in which significant radiators appear. The first peak occurs near 2.70 μ and corresponds to the so-called 2.7-μ bands. According to Goody (ref. 15), these bands are not fundamental CO_2 bands but do appear very strongly in the solar spectrum and consist of at least four combination bands of $C^{12}O_2^{16}$ and one of $C^{13}O_2^{16}$ in the spectral region 3613 - 3723 cm^{-1}. The second significant radiation band occurs between 4.2 and 5.0 μ and consists of the fundamental rotation-vibration band at 4.3 μ and the two groups of 5.0-μ bands indicated by Goody. It is interesting to note that the 2.0-μ, 1.6-μ, and 1.4-μ bands listed by Goody as much weaker bands do not appear as significant radiators.

The nonequilibrium radiation observed in this particular survey is shown in figure 9, where the ratio of peak nonequilibrium spectral intensity, G_{λ_p}, divided by equilibrium spectral intensity is shown for various wavelengths. A typical nonequilibrium overshoot is shown in the oscillogram in figure 7(a).

As figure 9 shows, nonequilibrium overshoot occurs at approximately 3.0 μ, and then again between 4.75 and 5.00 μ. In both spectral regions where nonequilibrium radiation occurs, the level of equilibrium radiation is much lower than the highest recorded values.

The results of the equilibrium radiation levels for the three higher velocity runs in different gas mixtures are shown in figures 9, 10, and 11. Figure 9 shows the equilibrium radiation levels behind incident shocks with average velocities of 15 268 fps into 1.0 mm Hg of CO_2. The general results are the same as described for the slower shock into 2.0 mm Hg CO_2; there are two general areas of significant radiation, corresponding to the 2.7-μ bands and a combination of the 4.3- and 5.0-μ bands. A finer resolution near 4.5 μ shows a dip in the peak that did not appear in the previous case when the resolution was not as good. The peak equilibrium radiation levels here are somewhat less than those corresponding to a slower shock speed, but this is to be expected because of the decrease in test gas density behind the shock front.

Figure 11 shows the effect of adding 1% N_2 to the gas mixture. The most noticeable influence is the disappearance of the equilibrium radiation near 2.70 μ. Another noticeable effect is the decrease in radiant intensity between 4.70 and 5.00 μ. Introduction of the 1% N_2 to an otherwise pure CO_2 test gas does not influence the radiant intensity of the fundamental 4.3-μ rotation-vibration band.

The effect of adding 20% A to the CO_2 is shown in figure 12. It is clear that the entire IR radiant intensity has been reduced. Again, the radiation from the 2.7-μ band has been almost completely extinguished, and that appearing between 4.2 and 5.0 μ has been reduced by a factor of two.

In figure 13, the nonequilibrium radiation observed for these three surveys is plotted as a ratio of G_{λ_p} to G_{λ_e}. Figure 13(a) shows the peak overshoot for a 100% CO_2 test gas; when compared to figure 9, which shows the same results for a slower initial shock velocity, it is clear that there is no essential difference in the nonequilibrium characteristics of the radiation, at least for these two velocities. That is, the nonequilibrium radiation that does occur appears in a spectral range where the total equilibrium radiation is already low compared to the peak equilibrium values. The largest peak overshoot occurs at 3.20 μ and is somewhat less than a factor of two times the equilibrium radiation. As shown in figure 10, the equilibrium radiation at 3.2 μ is much less than the peak value, which occurs near 4.4 μ. Here again, it should be pointed out that the 4.3-μ fundamental rotation-vibration band of CO_2 does not show a nonequilibrium overshoot for any of the three gas mixtures under these test conditions.

Peak nonequilibrium overshoots for the 99% CO_2 - 1% N_2 mixture are shown in figure 13(b). This mixture does show more overshoot than the pure CO_2 mixture, but again, it always occurs where the level of equilibrium radiation is much less than the recorded maximum values. Figure 13(c) shows the nonequilibrium radiation using the 80% CO_2 - 20% A mixture; note that the addition of argon to the test gas mixture does not have a significant influence.

Visible Spectral Survey

A complete spectral survey was obtained in the visible portion of the spectrum (2750 to 8500 Å) for each of the three different gas mixtures using initial average shock velocities near 14 600 fps. Typical oscillograph records obtained in these surveys are shown in records A, B, and C of figure 7. Each of these different records was obtained looking at a single event with different gain settings for the oscilloscope amplifiers.

Record 7(a) shows the large nonequilibrium overshoot behind a 15 030-fps initial shock into 1 mm Hg of 99% CO_2 - 1% N_2. The monochromator was set at 2750 Å for this shot and the spectral bandpass was 150 Å. The upper trace of this record could not be used because it goes off scale, but the lower trace does show a strong nonequilibrium overshoot, followed by a steady equilibrium value, which occurs some 2 μsec after shock arrival.

The traces shown in figures 7(b) and 7(c) are typical of the results obtained for the visible surveys in mixtures of 80% CO_2 and 20% A. In almost all of the visible records for this mixture, this type of double overshoot was observed; and in some cases [fig. 7(b)], the second overshoot was actually greater than the first. The first overshoot observed corresponds to shock arrival at the viewing ports and the second overshoot, which occurs approximately 5 μsec after shock arrival, is most probably a result of the delayed excitation of the argon atoms in the gas mixture. This type of delayed radiative phenomenon, using pure argon as the test gas under almost identical conditions, has been observed by Wong and Bershader (ref. 16), whose results correlate very closely with the delay time observed here. Wong and Bershader point out that the delay

is essentially the time required to produce a small number of electrons, followed by a cascading effect in which much higher degrees of ionization of argon occur, and that this corresponds to a strongly radiating flow.

To determine whether this second radiating front will contribute to the total radiative heat load of an entry body, one needs to know the shock standoff distance to determine if there is sufficient time for the phenomenon to occur. If the shock standoff distance is sufficiently large, the presence of argon in the gas mixture will give rise to a large number of free electrons, which could be of possible significance to the communication problem.

The equilibrium radiation results for the visible surveys of the different gas mixtures are shown in figures 14, 15, and 16. The gas behind the incident shock for these conditions is near 4000°K, and all the equilibrium data points lie below 1% of the black-body intensity, which indicates that self-absorption of the gas is negligible.

Figure 14 shows the equilibrium spectral radiant intensity for average shock velocities of 14 648 fps into a 1.0 mm Hg 100% CO_2 test gas. The radiation between 2750 and 2950 Å is probably due to the two very strong, persistent bands at 2883 and 2896 Å that result from the ionization of CO_2 to CO_2^+, according to Pearse and Gaydon (ref. 17). The strong radiation at 3100 and 3300 Å is the contribution from the many lines in the spectra of pure CO_2, which Pearse and Gaydon show, and the reduced intensity near 3200 Å corresponds to a relatively dark area in the CO_2 spectra. The lower intensity bands near 3900 and 4300 Å are probably the CO^+ comet tail bands mentioned by Pearse and Gaydon. The final significant points near 5000 Å correspond to the C_2 Swan band system, which has a band head at 5165 Å.

Figure 15 shows the results of adding 1% N_2 to the test gas mixture. It is clear that such a small amount of N_2 is not adequate to significantly change the appearance of the spectral radiation.

The results for an 80% CO - 20% A test gas mixture are shown in figure 16. As mentioned previously, the double overshoot of nonequilibrium radiation appears in almost all shots of this type. The equilibrium radiation levels were taken as those values behind the second peak. As shown in figure 7(b), the apparent equilibrium value recorded after the first overshoot is somewhat lower than the final equilibrium value behind the second overshoot. This type of approach to equilibrium is consistent with the discussion given by Wong and Bershader (ref. 16). As they point out, the argon plasma actually reaches equilibrium after the free bound radiation following the cascading effect in the production of free electrons.

The ratio of peak nonequilibrium to equilibrium visible radiation for the three gas mixtures is shown in figure 17. Note that the ratio is generally less than two. Both the 100% CO_2 mixture and the 80% CO_2 - 20% A mixture show an overshoot at 0.30 μ (where the peak radiative intensity occurs), but the 99% CO_2 - 1% N_2 mixture does not have an overshoot in this spectral region.

Variation of G_{λ_e} with Initial Pressure

A limited number of experiments have been conducted to determine the variation of equilibrium radiant intensity with density. These tests were conducted at a constant initial shock velocity of 13 607 fps at 3425 Å in a test gas mixture of 99% CO_2 and 1% N_2. The results (fig. 18) show that G_{λ_e} increases with increasing density behind the normal shock front. This trend is in accord with the theory, which holds that the spectral radiance for a transparent gas is directly proportional to the number density.

CONCLUSIONS

The spectral radiative intensity has been measured under various test conditions for three different candidate Mars atmospheres over the wavelength range from 0.275 to 5.0 μ. The IR portion of the spectral radiation for all three gas mixtures tested shows a peak in intensity between 4.3 and 5.0 μ corresponding to the fundamental rotation-vibration band of CO_2 and the 5.0-μ bands of CO_2. The 100% CO_2 test gas also shows a strong band radiation at 2.7 μ. This strong peak is greatly reduced when either nitrogen or argon is added to the test gas mixture. The nonequilibrium radiation that appears in the IR always occurs in those spectral regions for which the equilibrium levels are lowest. It is especially interesting to note that no nonequilibrium radiation was associated with the fundamental 4.3-μ band of CO_2 in either of the test gas mixtures.

One very interesting feature of the visible radiation spectrum is the double nonequilibrium overshoot, which is characteristic of the test gas mixture containing argon. This phenomenon has been observed in previous experiments dealing with argon plasmas and is a very likely source of a significant number of free electrons.

In general, the nonequilibrium radiation from these gas mixtures behind shock waves with velocities up to 16 000 fps is much less than that observed in mixtures containing larger amounts of nitrogen. Maximum observed nonequilibrium overshoots occur in the visible portion of the spectrum and are generally no larger than two times the equilibrium value. The major portion of both the IR and the visible spectrums have nonequilibrium overshoots less than 1.5 times the equilibrium values.

Martin Marietta Corporation,
Denver, Colorado, July 22, 1970

REFERENCES

1. Boobar, M. G.; and Foster, R. M.: Some Aerothermodynamic Considerations for Martian Entry and Heat Shield Design. IAS Paper 62-163, 1963.

2. James, Carlton S.: Experimental Study of Radiative Transport from Hot Gases Simulating in Composition the Atmosphere of Mars and Venus. AIAA J., vol. 2, 1964, pp. 470-475.

3. Fairbairn, A.: The Spectrum of Shock-Heated Gases Simulating the Venus Atmosphere. AIAA Paper 63-454, 1967.

4. Gruszczynski, J. S.; and Warren, W. R., Jr.: Experimental Heat Transfer Studies of Hypervelocity Flight in Planetary Atmospheres. AIAA J., vol. 2, 1964, pp. 1542-1550.

5. Thomas, G. M.; and Menard, W. A.: Experimental Measurements of Nonequilibrium and Equilibrium Radiation from Planetary Atmospheres. AIAA J., vol. 4, 1966, pp. 227-237.

6. Arnold, J. O.; Reis, V. H.; and Woodward, H. T.: Studies of Shock-Layer Radiation of Bodies Entering Planetary Atmospheres. AIAA J., vol. 3, 1965, pp. 2019-2025.

7. Rumpel, W. F.; and Deacon, H. J., Jr.: Additional Conclusion on the Energy of Formation of CN. J. Astro-Sci., vol. XV, No. 4, July-Aug. 1968, p. 207.

8. Reis, V. H.: Oscillator Strength of the CN Violet System. JQSRT I, No. 585, 1965.

9. Gruszczynski, J. S.: Experimental Investigations of Self-Absorption and Vacuum UV Molecular Radiation in Simulated Planetary Atmospheres. AIAA Paper 68-655, 1968.

10. McKenzie, R. L.; and Arnold, J. O.: Experimental and Theoretical Investigations of the Chemical Kinetics and Nonequilibrium CN Radiation Behind Shock Waves in CO_2-N_2 Mixtures. AIAA Paper 67-322, 1967.

11. Menees, G. P.; and McKenzie, R. L.: A Simplified Chemical Model for Estimating the Nonequilibrium Radiant Emission of CN (Violet) in Shock-Heated Mixtures of CO_2 and N_2. AIAA J., vol. 6, 1968, pp. 554-556.

12. Menard, W. A.; and Thomas, G. M.: Radiation Measurement Techniques. Technical Report No. 32-975, Jet Propulsion Laboratory, Pasadena, California, Aug. 1966.

13. Stair, R.; Johnston, R. G.; and Halbach, E. W.: Standard of Spectral Radiance for the Region of 0.25 to 2.6 Microns. J. Res. NSS 64A, July-Aug. 1960, p. 291.

14. Gillespie, R. E.; Avrin, P.; and Ress, E. B.: Parabolic Reflectometer Description, Evaluation, and Preliminary Measurement Investigation. Report No. 1610-68-43, Martin Marietta Corporation, Denver, Colorado, Nov. 1968.

15. Goody, R. M.: Atmospheric Radiation. Oxford University Press, 1964, pp. 207-209.

16. Wong, H.; and Bershader, J.: Thermal Equilibration Behind an Ionizing Shock, J. Fluid Mech., vol. 26, No. 459, 1966.

17. Pearse, R. W. B.; and Gaydon, A. G.: The Identification of Molecular Spectra. Chapman & Hall, Ltd., 1963, p. 123.

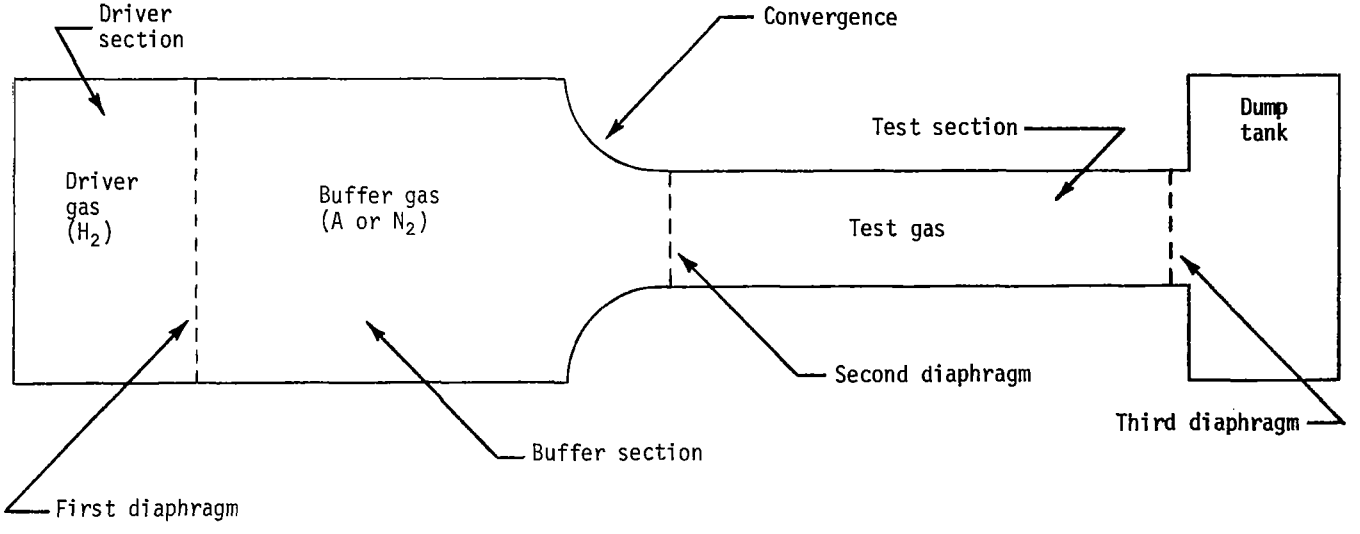

Figure 1.- A Chambered Buffer Shock Tube

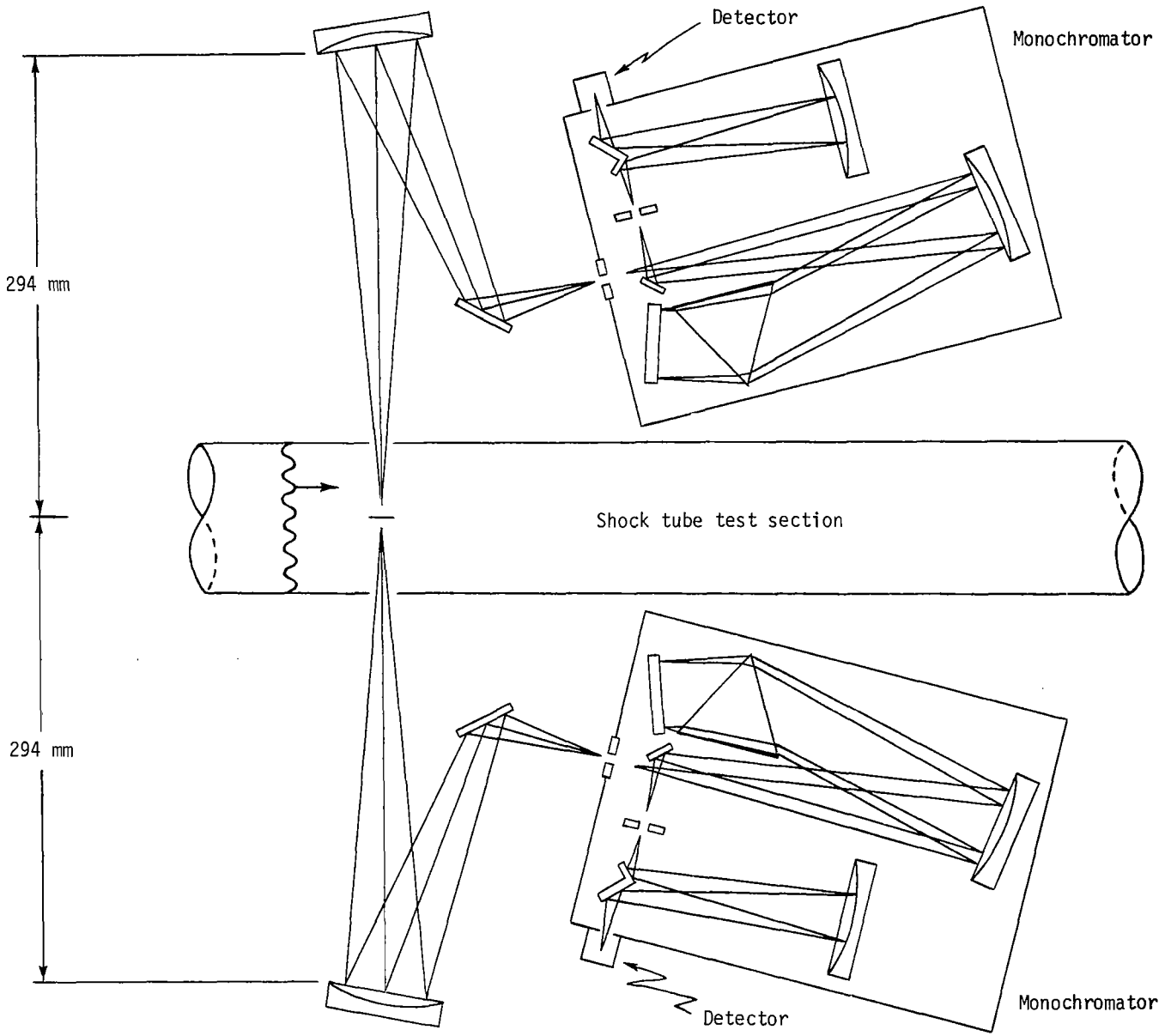

Figure 2.- Experimental Setup

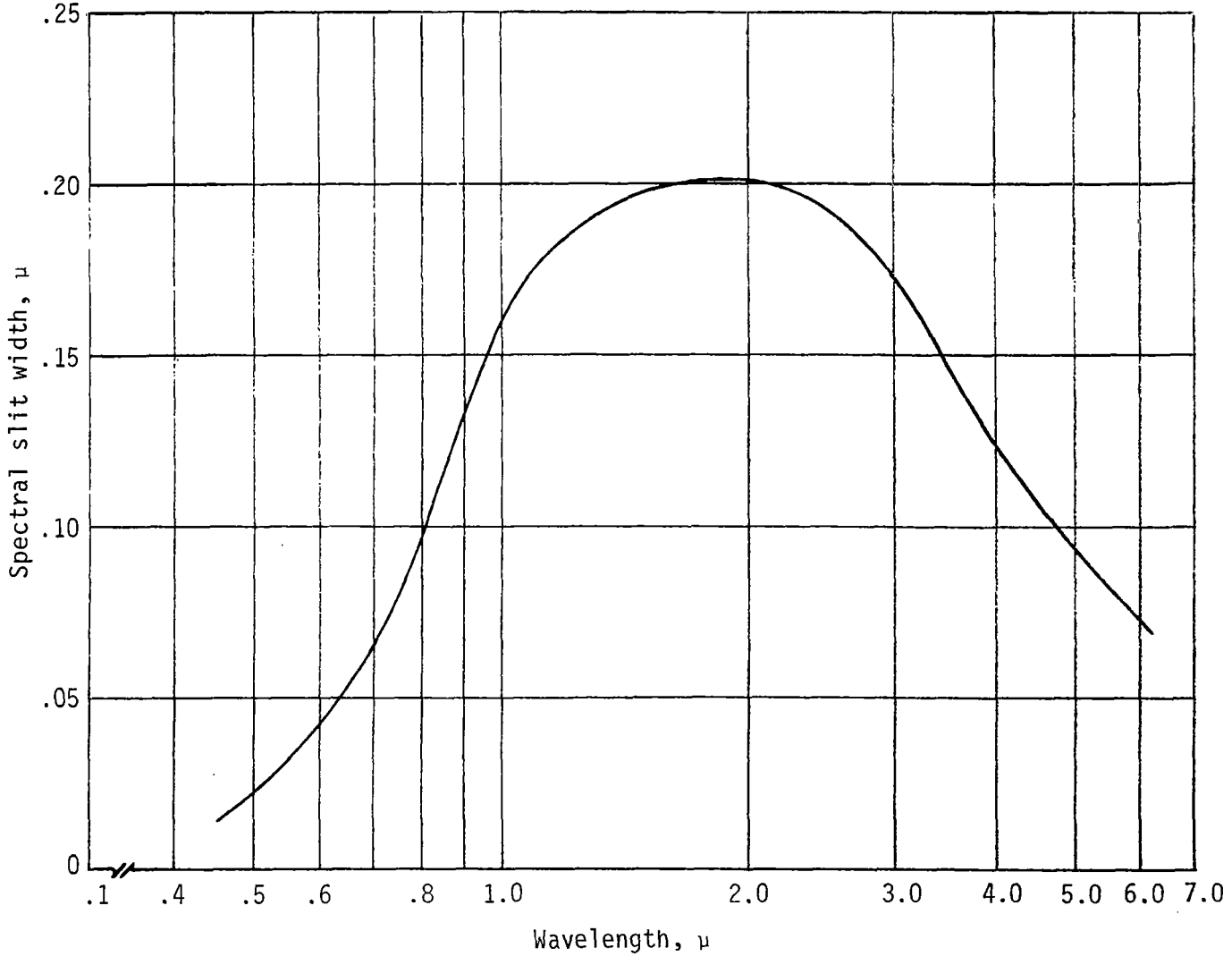

Figure 3.- CaF_2 Spectral Slit Width for 1-mm Physical Slit Width

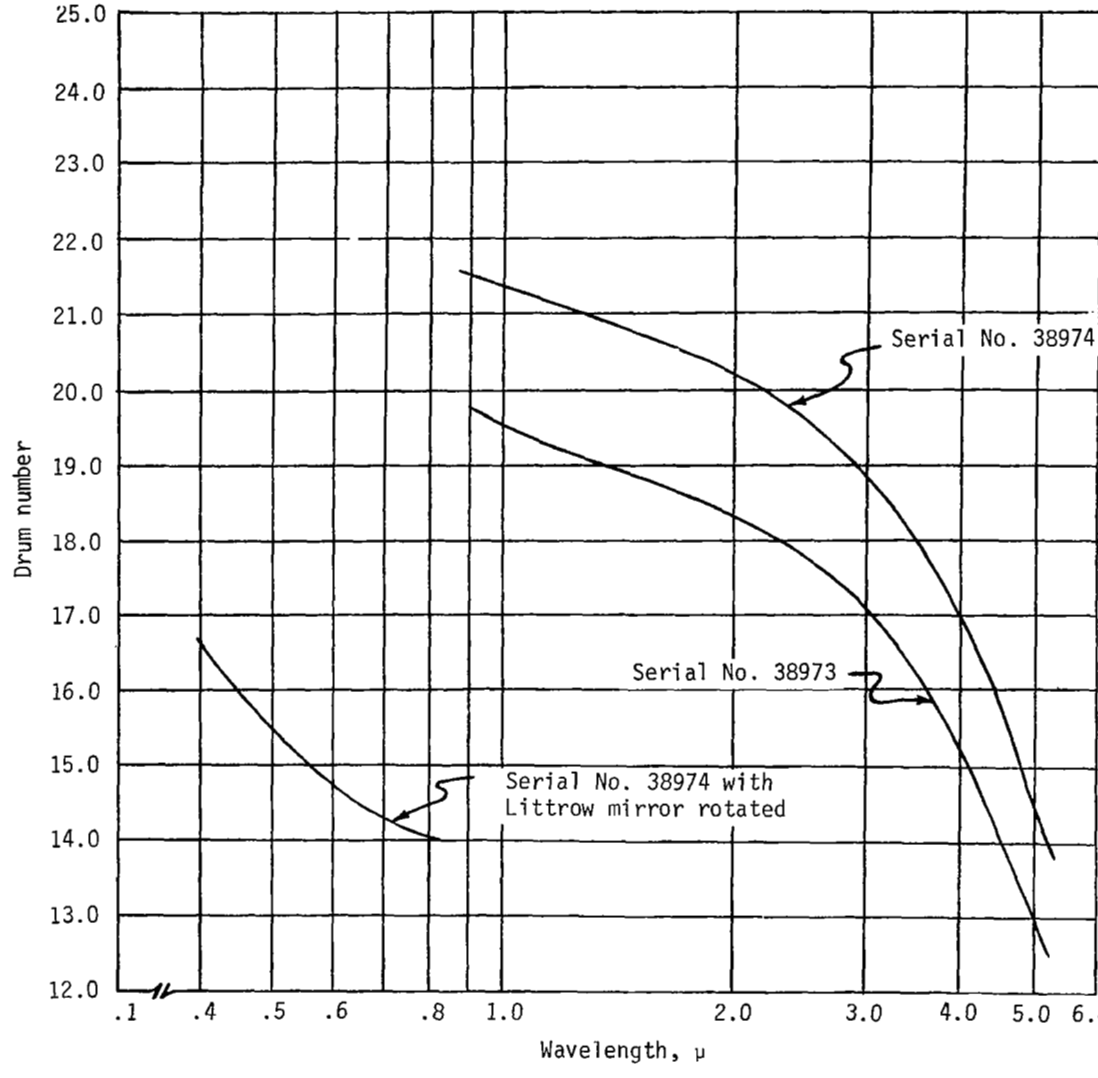

Figure 4.- Drum Number vs Wavelength

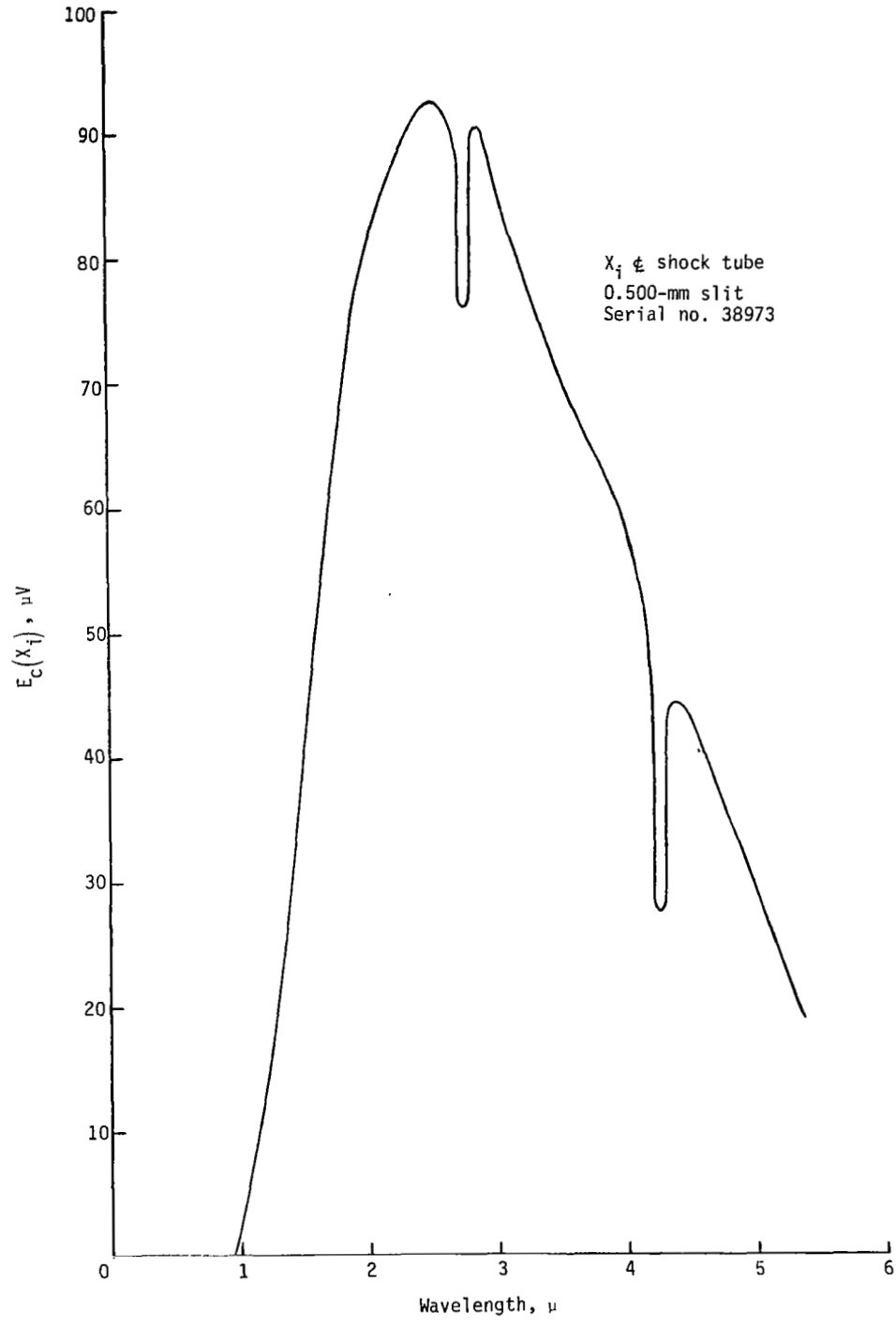

Figure 5.- $E_c(X_i)$ vs Wavelength

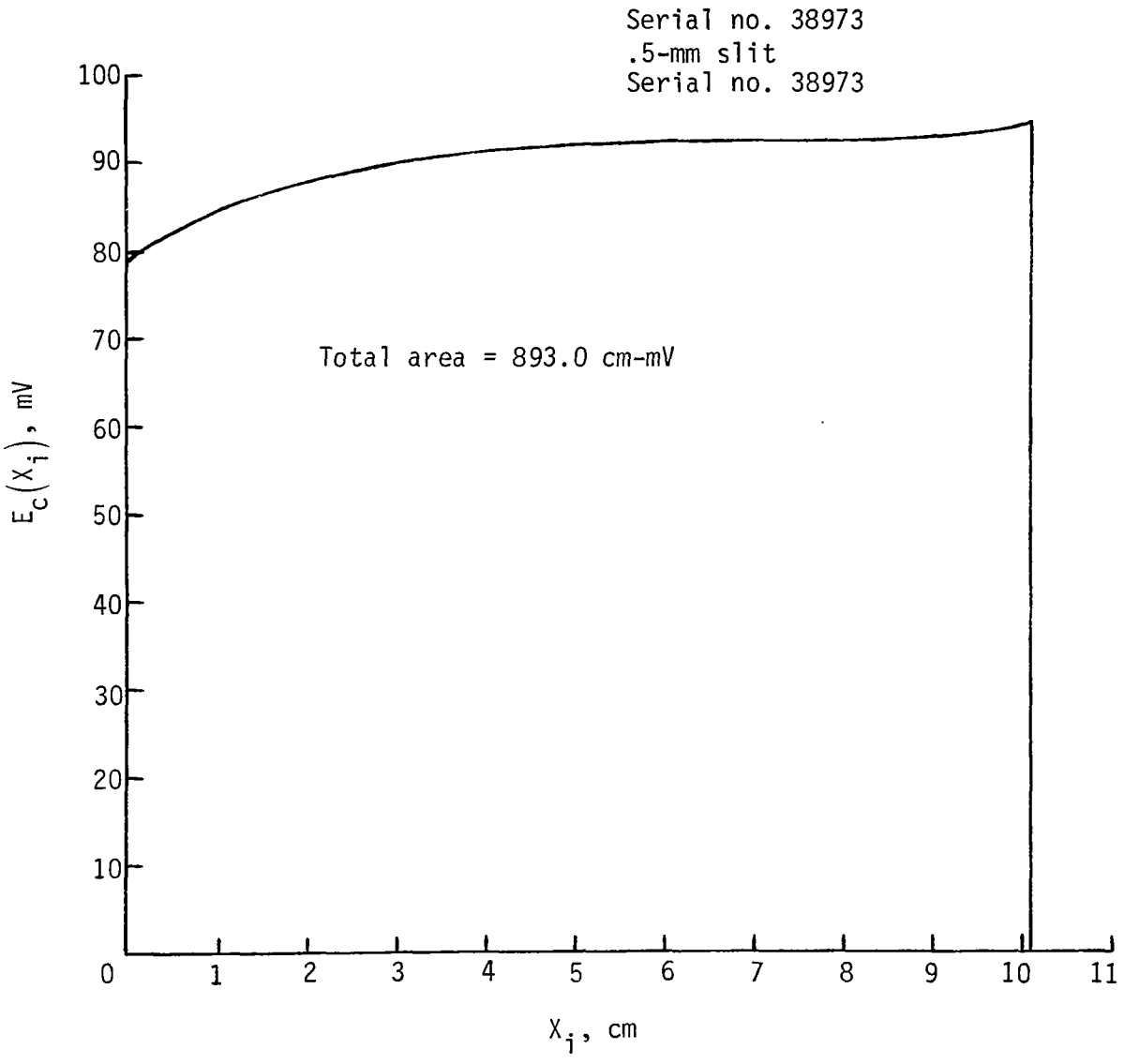

Figure 6.- $E_c(X_i)$ vs X_i at λ = 2.50 μ

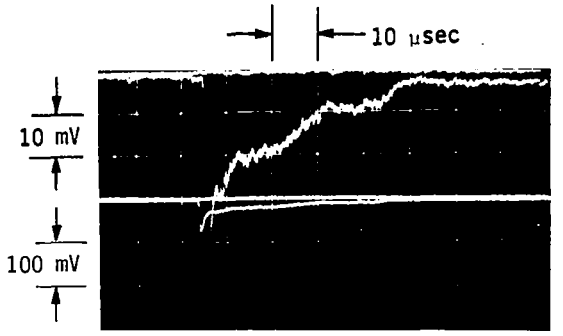

(a) 99% CO_2 - 1% N_2, P_1 = 1 mm Hg, V_s = 15 030 fps, λ = 2750 Å

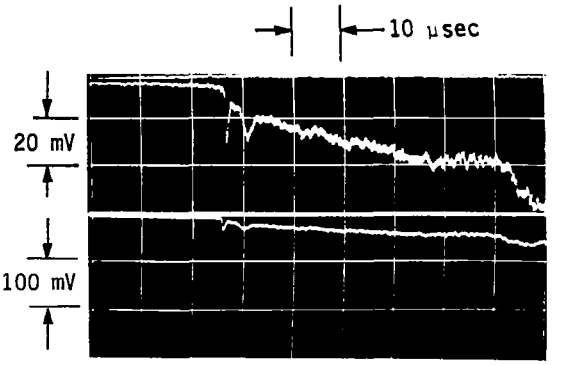

(b) 80% CO_2 - 20% A, P_1 = 1 mm Hg, V_s = 14 151 fps, λ = 7100 Å

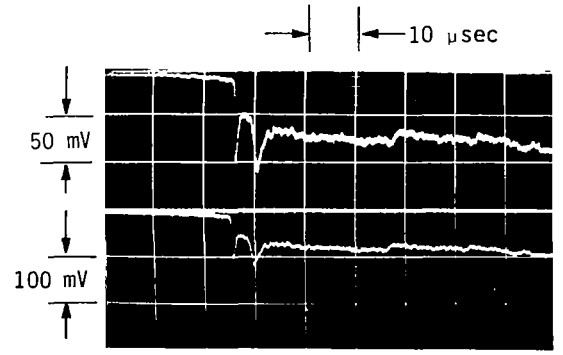

(c) 80% CO_2 - 20% A, P_1 = 1 mm Hg, V_s = 14 368 fps, λ = 6200 Å

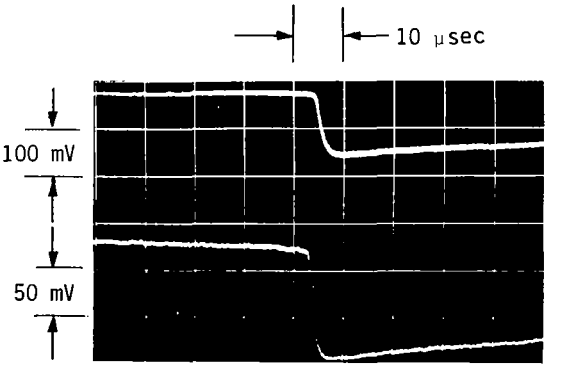

(d) 100% CO_2, P_1 = 2 mm Hg, V_s = 12 864 fps, λ = 4.26 μ

Figure 7.- Typical Oscillograph Records

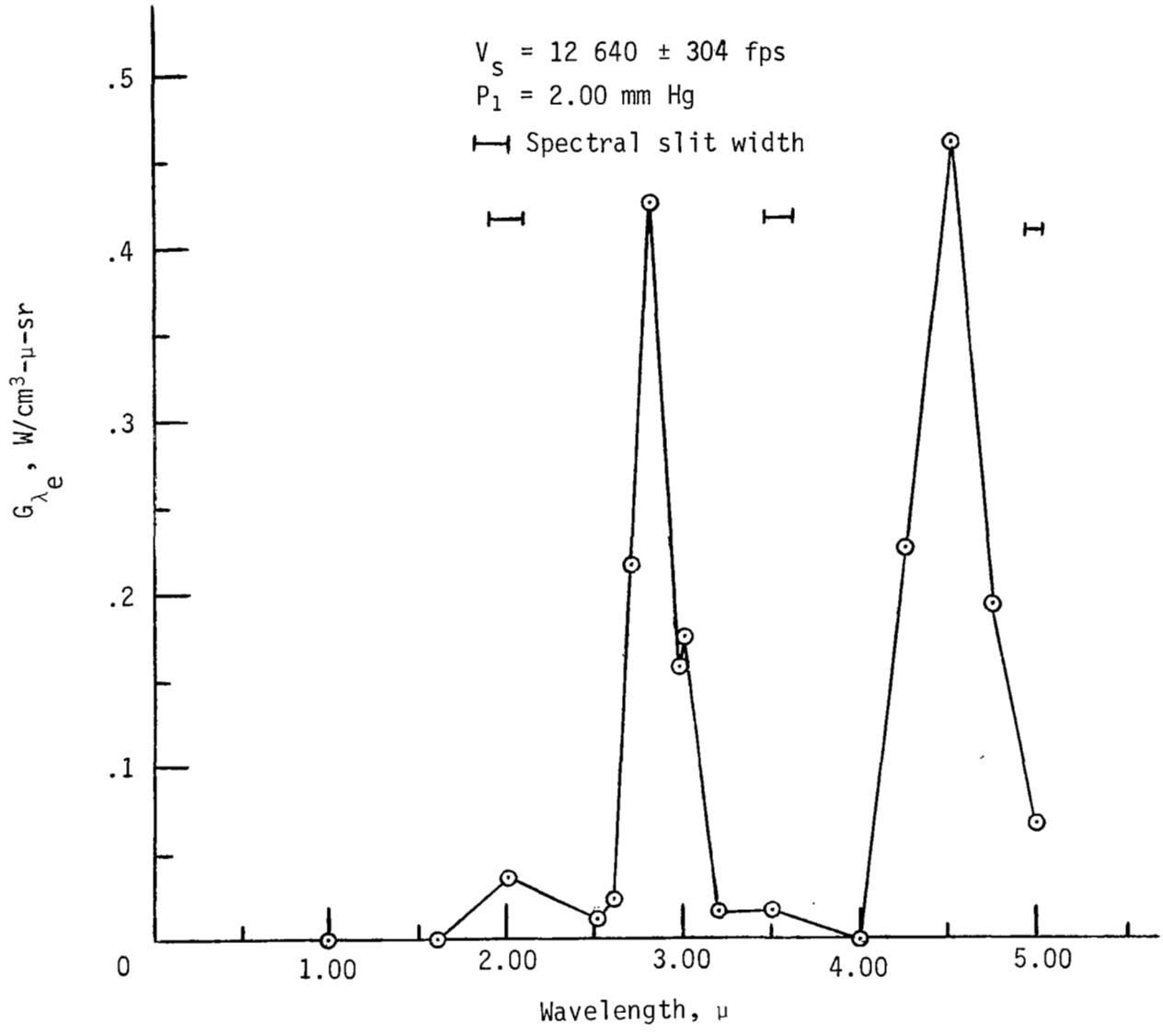

Figure 8.- Equilibrium Radiation Behind the Incident Shock for 100% CO_2

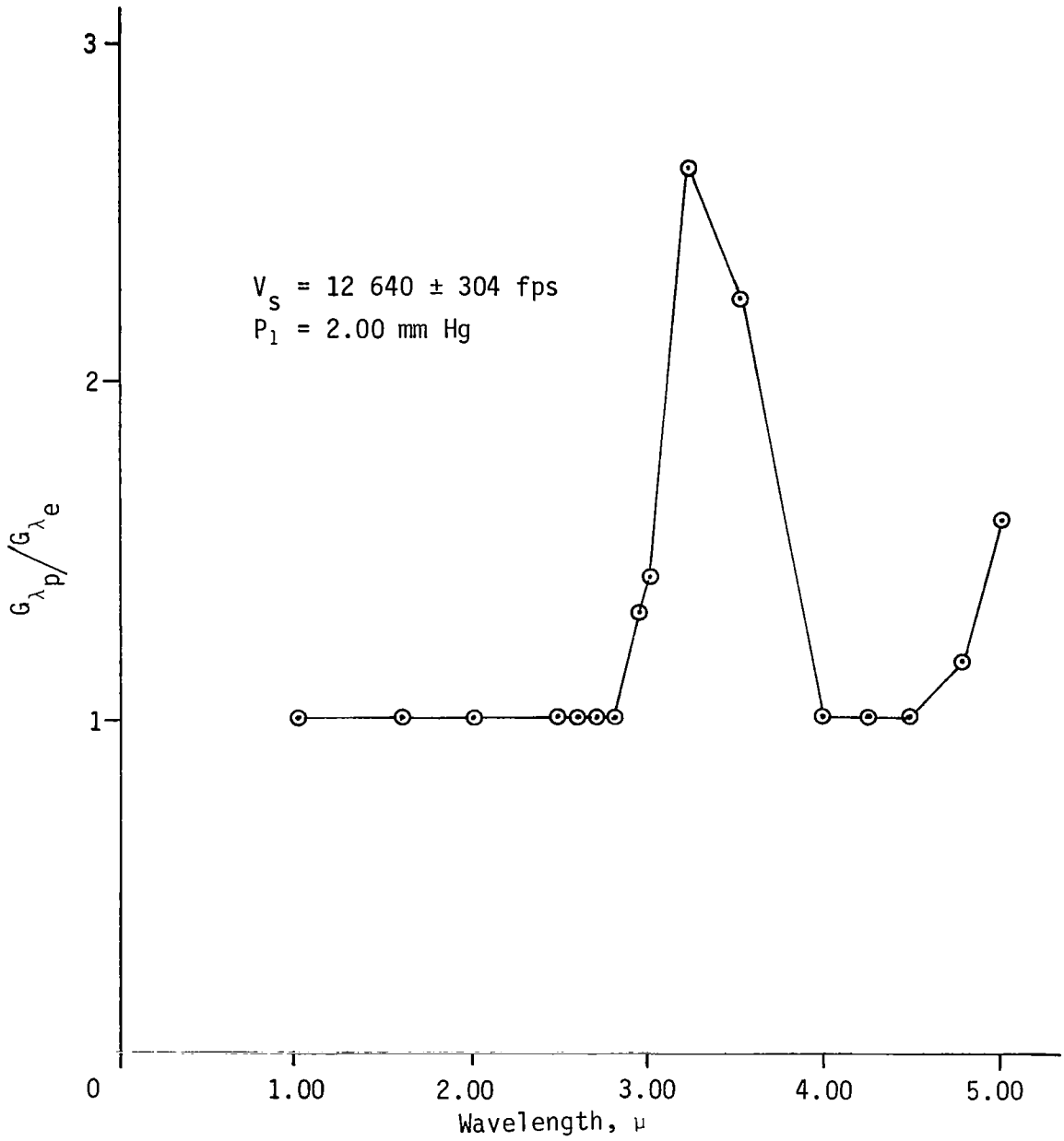

Figure 9.- Ratio of Nonequilibrium to Equilibrium Radiation Behind Incident Shock for 100% CO_2

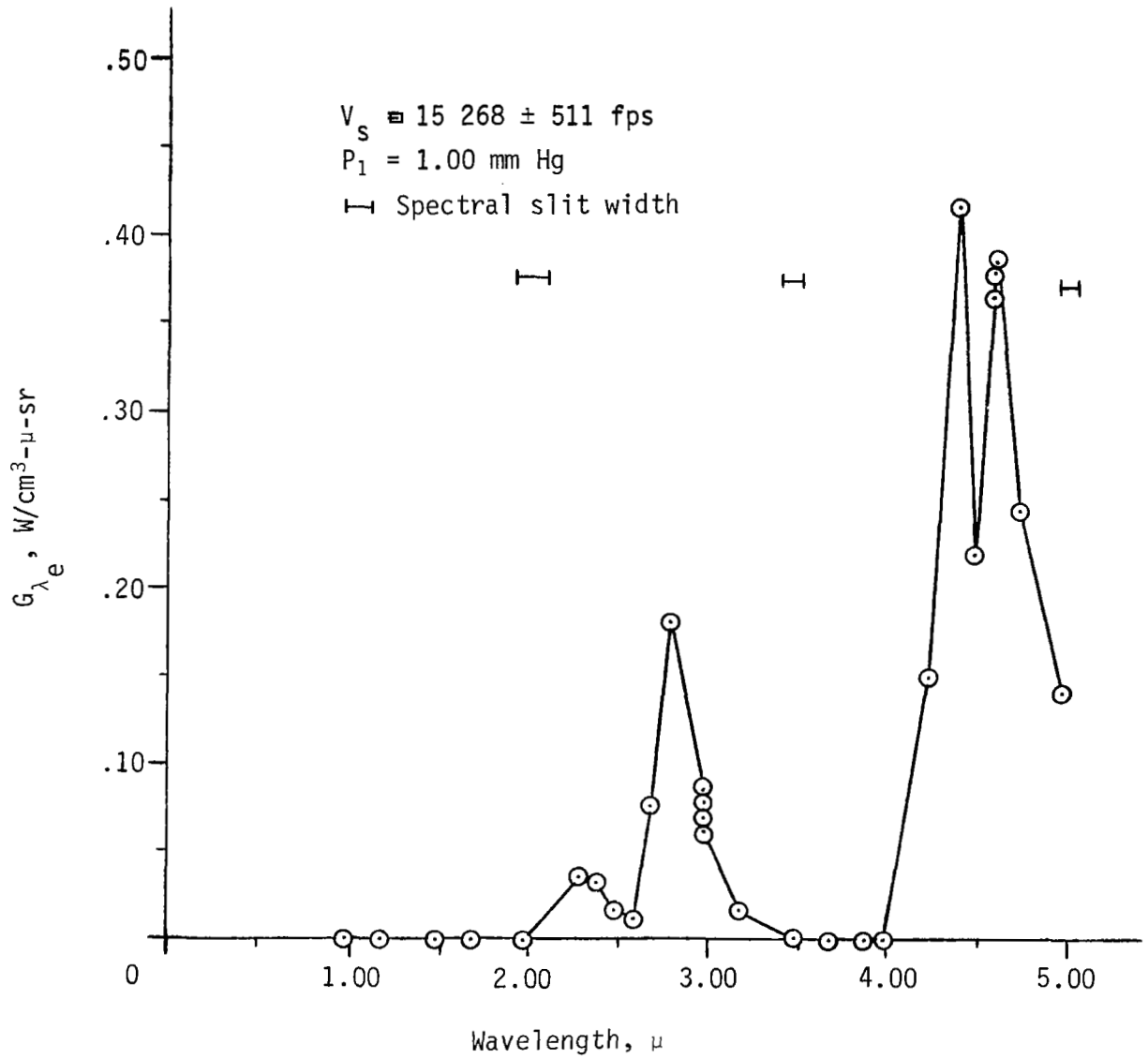

Figure 10.- Equilibrium Radiation Behind the Incident Shock for 100% CO_2

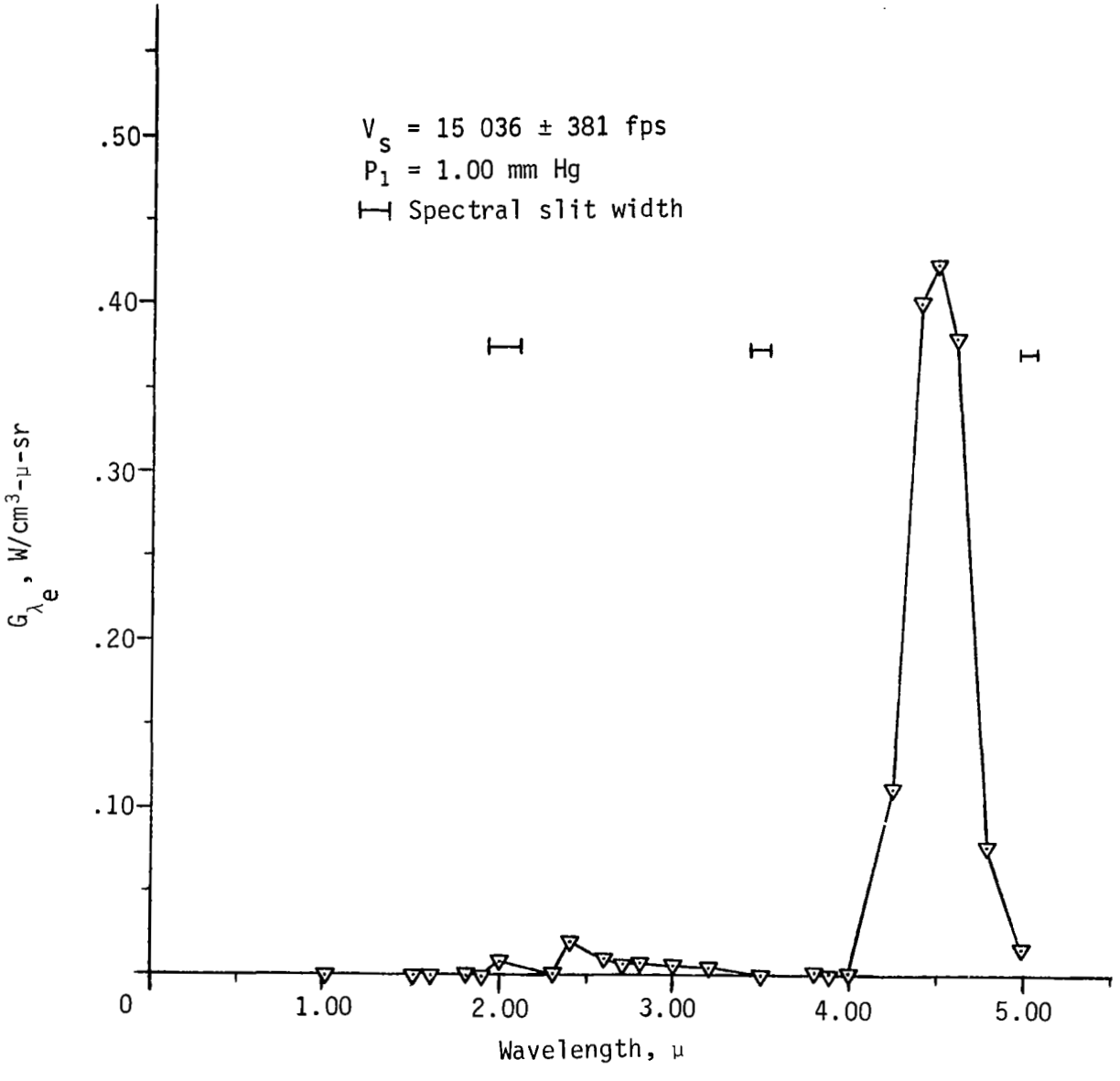

Figure 11.- Equilibrium Radiation Behind the Incident Shock for 99% CO_2 - 1% N_2

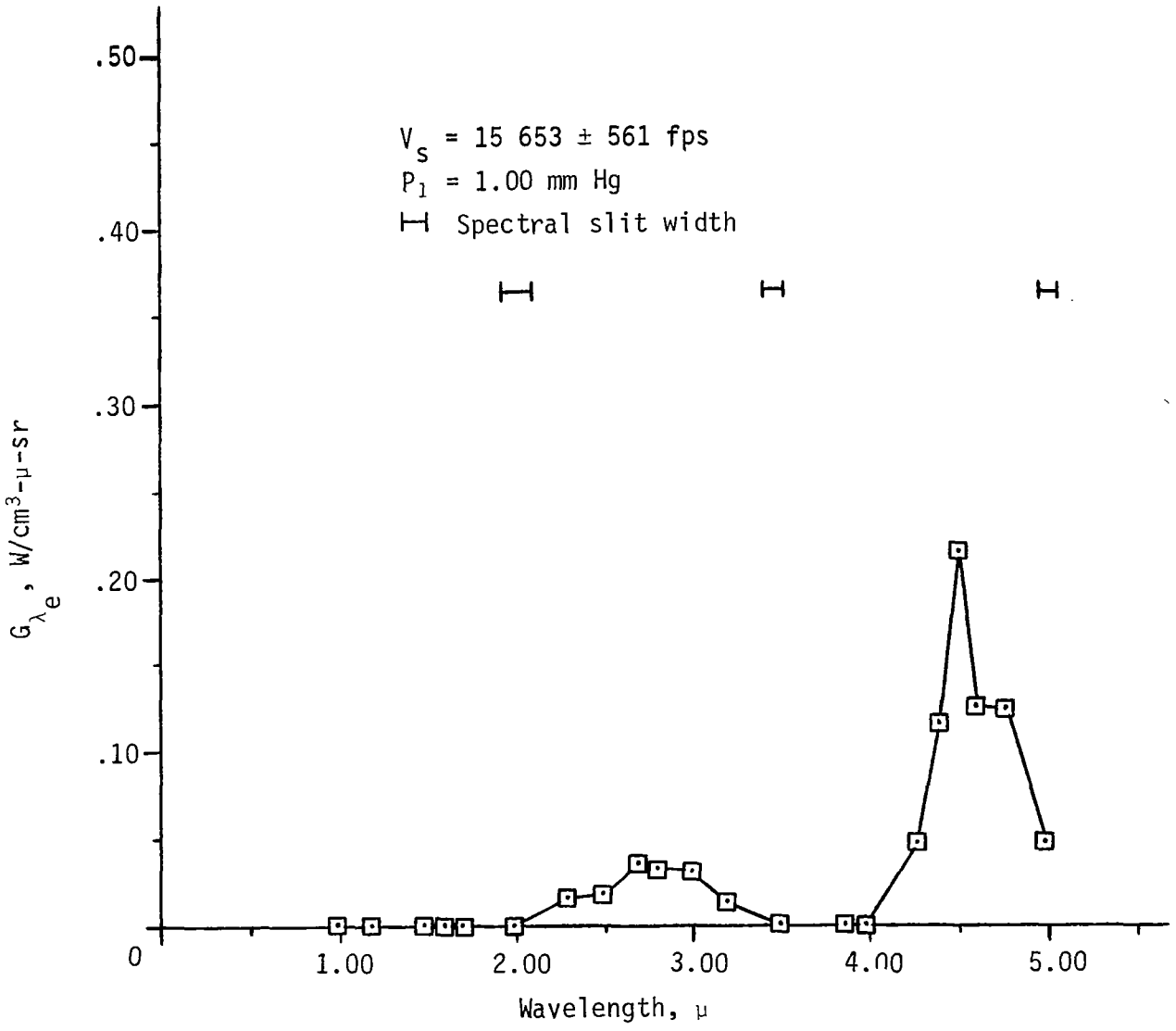

Figure 12.- Equilibrium Radiation Behind the Incident Shock for 80% CO_2 - 20% A

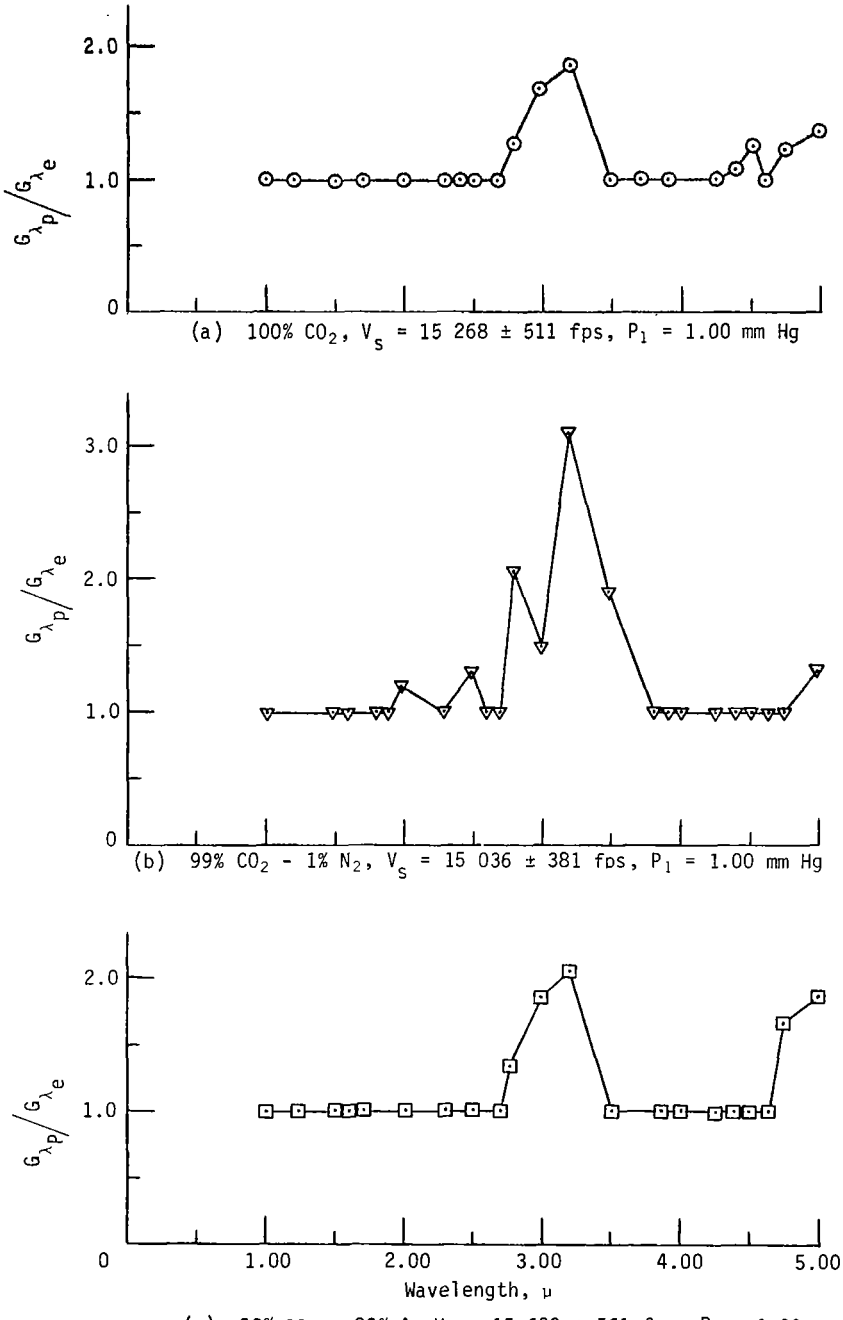

Figure 13.- Ratio of Nonequilibrium to Equilibrium Radiation for Different Test Gas Mixtures

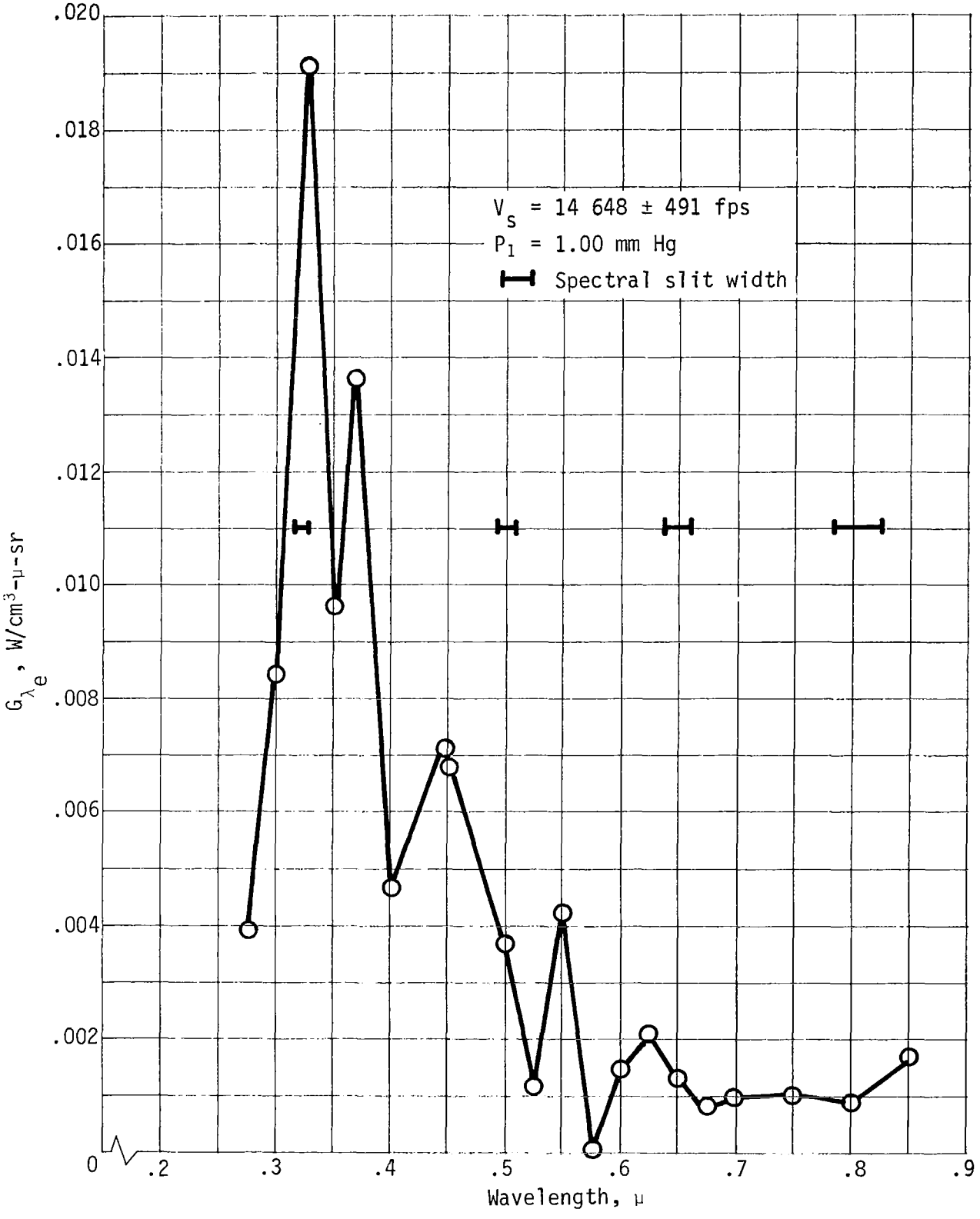

Figure 14.- Equilibrium Radiation Behind an Incident Shock in 100% CO_2

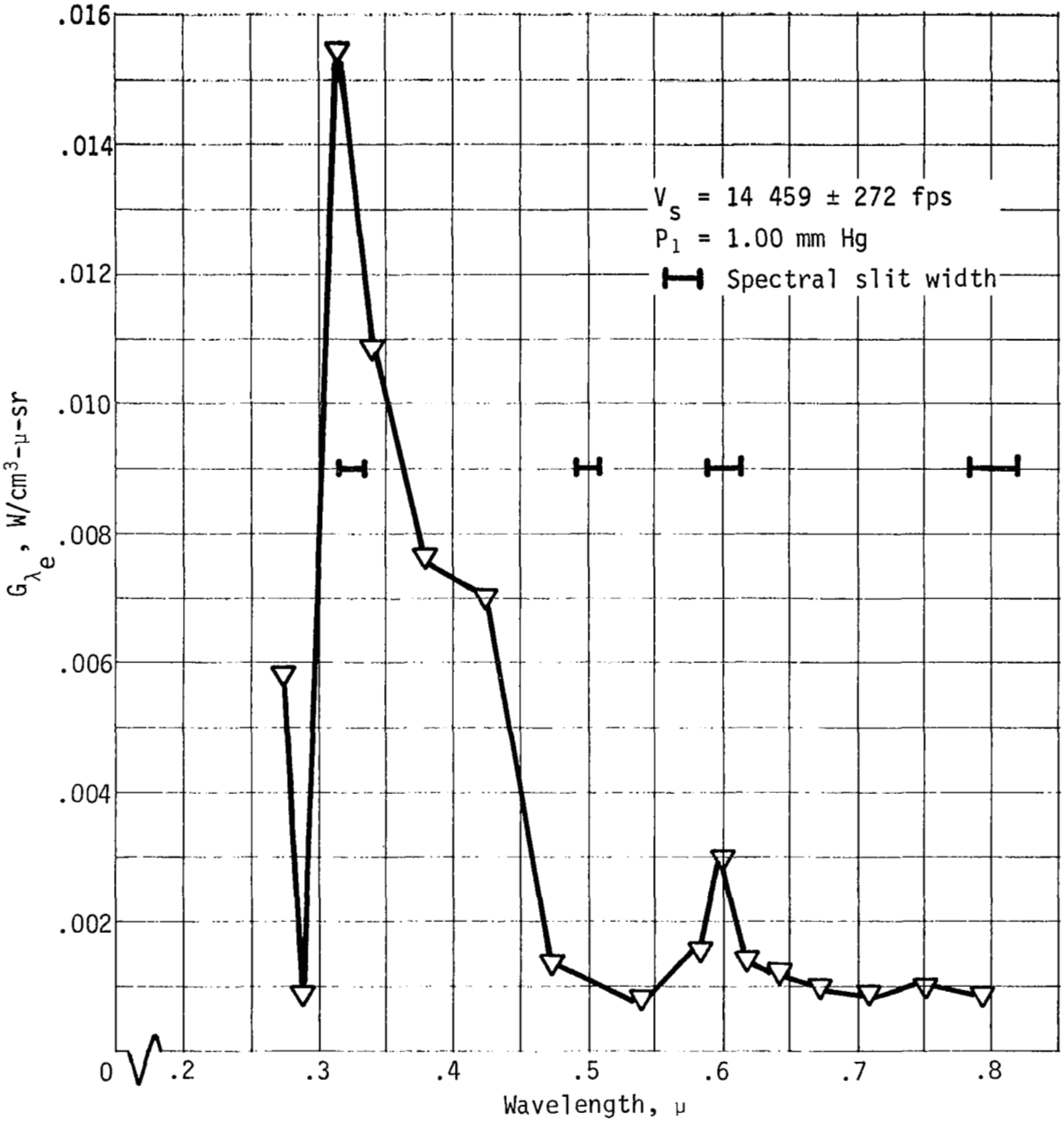

Figure 15.- Equilibrium Radiation Behind an Incident Shock in 99% CO_2 - 1% N_2

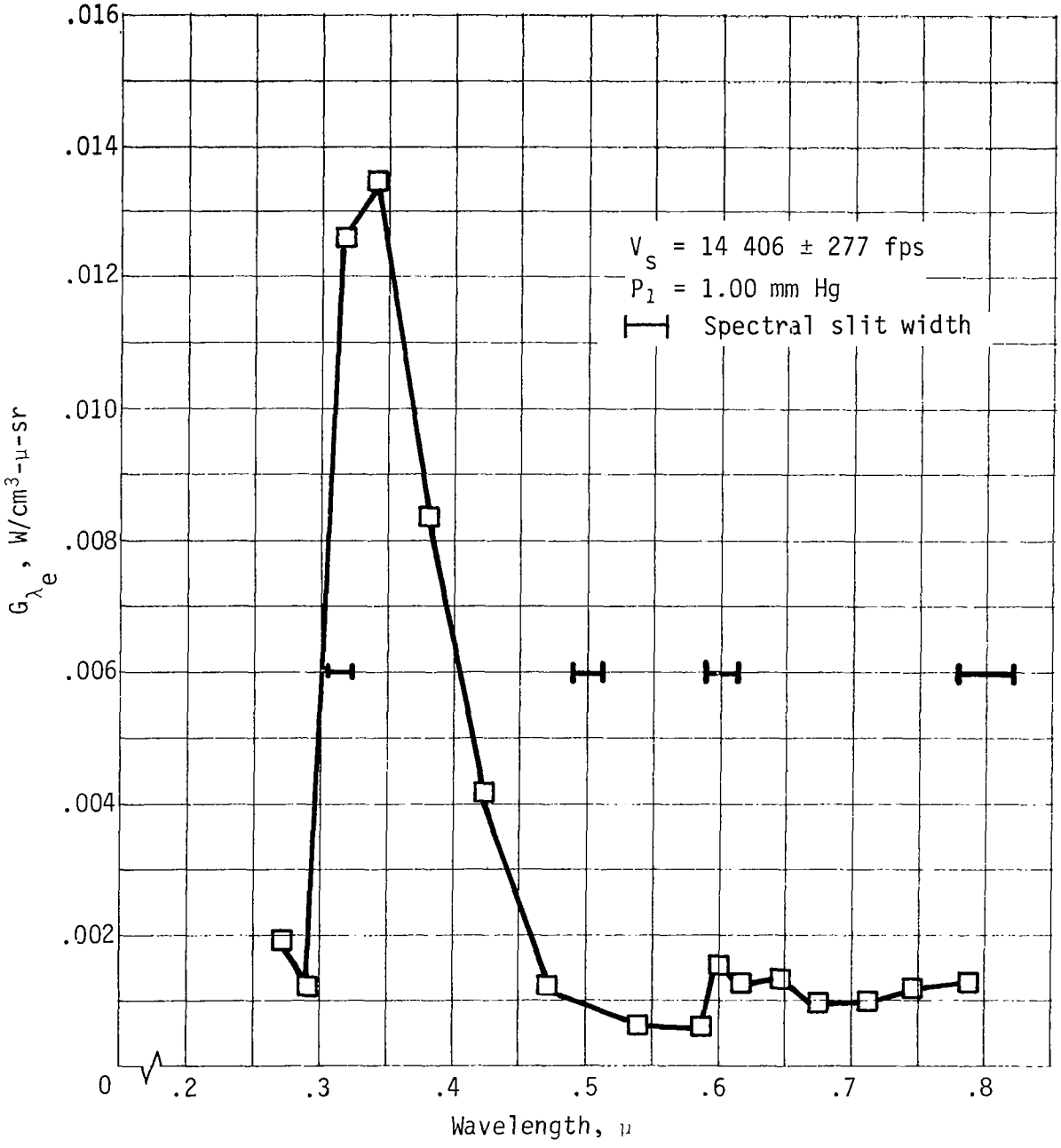

Figure 16.- Equilibrium Radiation Behind an Incident Shock in 80% CO_2 - 20% A

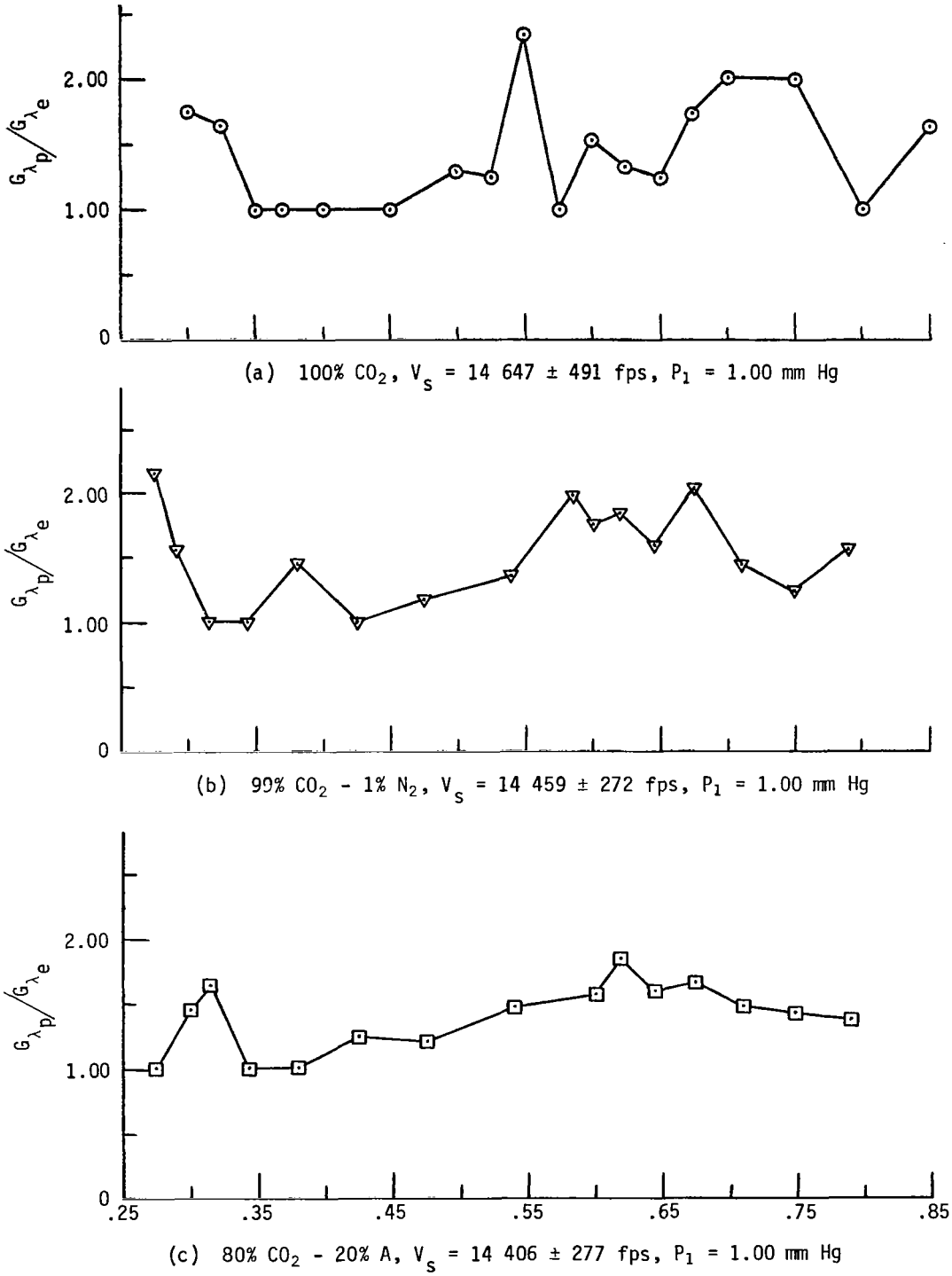

Figure 17.- Ratio of Nonequilibrium to Equilibrium Radiation for Different Test Gas Mixtures

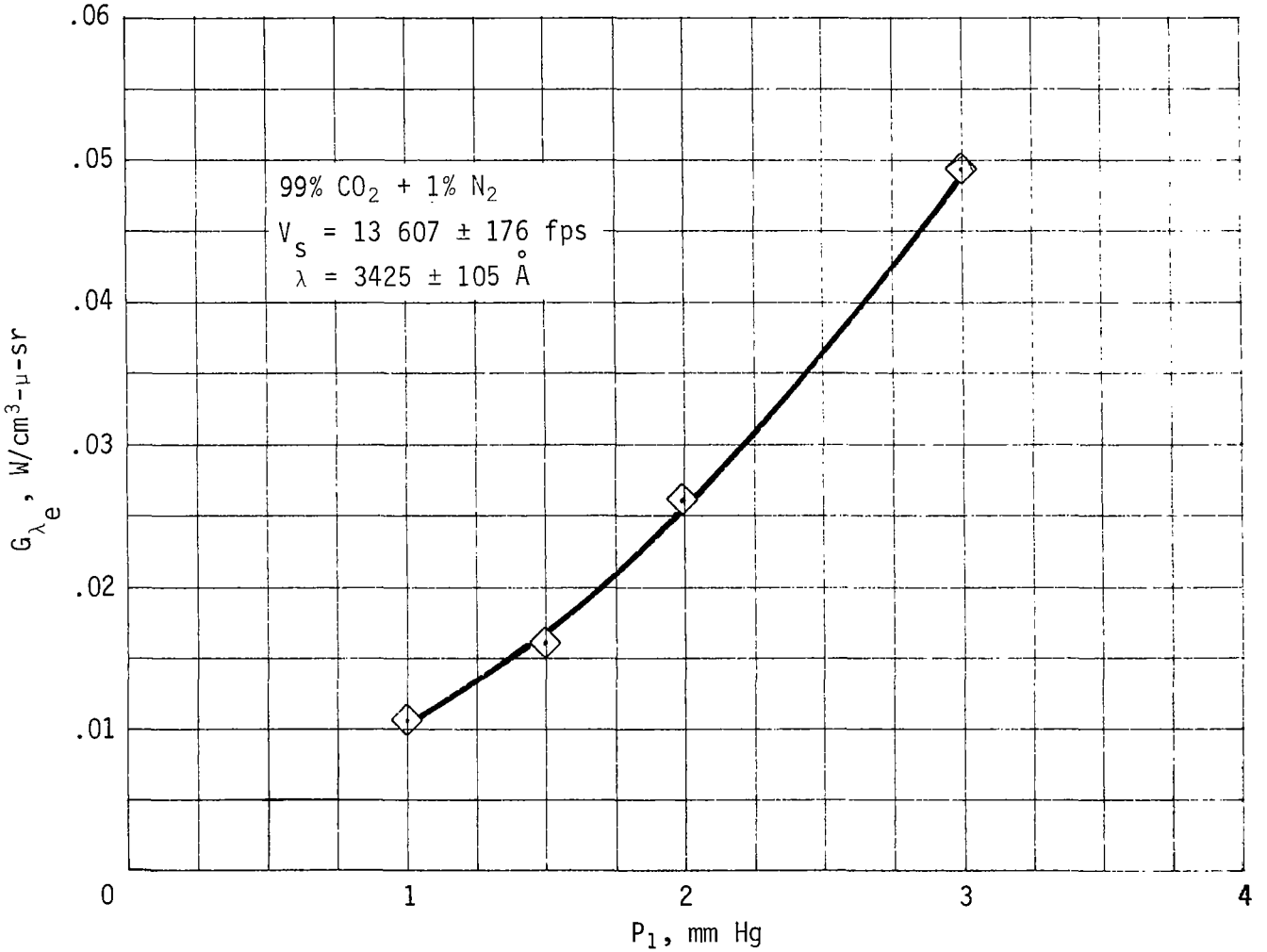

Figure 18.- Variation of G_{λ_e} with P_1